Journal of New Technology and Materials (JNTM)
J. New Technol. Mater.
Vol. 10, N°01 (2020)63-68

OEB Univ. Publish. Co.

Microstructural characterization, mechanical properties and recrystallization kinetics of low carbon steel wires

Z. Larouk[a], A. R. Khantoul[b], A. Ayad[a,c,*] and H. Bouhalais[a]

[a]*Laboratory of Microstructures and Defects in materials, University Frères Mentouri Constantine 1, Ain El Bey way, Constantine 25017, Algeria*

[b]*Laboratory of Crystallography, University Frères Mentouri Constantine 1, Ain El Bey Way, Constantine 25017, Algeria*

[c]*Departement of Pharmacy, Faculty of Medecine, University Salah Boubnider Constantine 3, New Town of Ali Mendjeli, Constantine 25005, Algeria*

*Corresponding author, email: abdelhak.ayad@univ-constantine3.dz

Received date: Mar. 18, 2020; revised date: May 10, 2020; accepted date: May 13, 2020

Abstract

The present study deals with two steel wires containing different amount of carbon. The optical and Secondary Electron microscopy (SEM) are used to identify the microstructure of steels in as-received and deformed conditions. The results show that the mechanical and structural properties are affected by the carbon content. It is found that the kinetics of primary recrystallization is described by Avrami law at 500°C and the rate of primary recrystallization depends on carbon content. The two parameters (k and n) in Avrami law are calculated and the activation energy for primary recrystallization is found to be lower for the low carbon content steel.

Keywords: Low carbon steel; wiredrawing; primary recrystallization; kinetics; *activation energy*

1. Introduction

Mechanical and structural properties of steel are influenced by many parameters as density dislocations, grain size and grain orientation and chemical composition [1-5]. However, it is well known that the amount of alloying elements in solid solution and ferrite grain size exert a significant influence upon the microstructure of steels. The carbon content has a very strong effect on the steel strength since it controls the amount of cementite present in steels.

The interaction of dislocations with the interstitial atoms, such as carbon and nitrogen, reveal the presence of yield-point phenomena in soft steel. Carbon and nitrogen atoms diffuse to the core of dislocations and oppose their motion which results in the increasing of hardening [1].

Inclusions are always present in the steels since are the product of casting process. It is well known that their presence has a bad effect on wire steel strength during wiredrawing process by limiting the final reduction of area [3]. The weak link between inclusions and matrix acts as preferable sites for micro cracks nucleation and growth. The most important consequence of a deformed microstructure is the increase of the dislocation density. This is the major strengthening mechanisms of alloys [6]. If any alloy containing a second phase precipitates (or inclusions), with low mechanical properties, dislocations cross these particles and deform them; while particles (or inclusions), with high mechanical properties, dislocations bend them which results in an increase in dislocation density.

Secondary Electron Microscope (SEM) is an important tool for the examination of the fractured surface and the determination of the failure cause. Dimple rupture represents ductile fracture, which thought to occur by nucleation of voids followed by either the coalescence or propagation of cracks between them. During wiredrawing, hard inclusions and also the interface inclusion/matrix may break. The latter is considered to be the most critical sites because of the high stress concentration in this interface [3].

Hardening by plastic deformation is an important method for strengthening alloys. During the wiredrawing process a considerable amount of energy is expended. Most of this energy goes into heat, but a less fraction of it remains in the steel as stored energy. The plastic deformation of steel causes the grains to become elongated. The elongated grains result in unstable structure. An optimal annealing allowed a return to a stable condition by progressive eliminating of stocked deformation energy. The annealing processes involve the migration of internal grain boundaries within the deformed material and the production of a new equiaxed grain structure. This process is termed recrystallization [7]. The formation of a new grain structure could be inhomogeneous and is attributed to the heterogeneous distribution of nucleation sites and the stored energy. Shear bands, grain boundaries and triple points are found to be the preferential nucleation sites [8].

The primary recrystallization rate is strongly depending on the chemical composition, the temperature and time of annealing. Ferrite grain refinement, obtained after complete recrystallization, is an important objective of low carbon steels; since it ensures a balance between high strength and good toughness [9].

The present study attempts to examine the combined effect of chemical composition and the rate of deformation on the microstructure and its mechanical properties of steel wires, in as received condition and after deformation. It is also devoted to estimate the kinetics of primary recrystallization and activation energies of steel wires.

2. Experimental procedure

The investigated material was low carbon steel wires supplied by the "Trifisoud, Setif, Algerie". The first steel was referred as S1 and the second as S2. The material was received in two different long rods with diameters of 6 mm (S1) and 5.5 mm (S2), then were formed at room temperature to a final diameters of 3.18 mm (S1) and 3.25 mm (S2), equivalent to wiredrawing area reduction of 72% and 65% respectively. The chemical composition of the steels is shown in table (1).

Table 1: Chemical composition (weight %)

Steel	C	Si	Mn	P	Cu	S	Cr	Ni	Mo
S1	0.05	0.10	0.30	0.02	0.12	0.025	0.12	0.12	-
S2	0.12	0.09	0.42	0.03	0.36	-	0.03	0.18	0.02

It is necessary to point out that the differences in alloying elements and the wiredrawing area reduction were given by "Trifisoud" plant and it is not possible to suggest a special chemical composition or a determined deformation rate.

The material was formed using a wiredrawing machine BREITENBACH type Standard 1R/4VZ. The process was carried out at room temperature using a soap of silicate as a lubricant.

Both steels, in as received condition, were subjected to dilatometer test. The sample was heated up to 1000 °C under Argon atmosphere. The heating and cooling rates were equal to 3 °C/min. The dilatometer used was ADAMEL L'HOMERGY DI 24 type.

Optical metallographic examination, using a ZEISS microscope equipped with AXIO-VISION software used for image analysis, was carried out on samples after grinding, polishing and etching in a solution of 2% concentrated nitric acid in ethanol. The polished samples were also used for hardness measurements, which were made using a Vickers hardness testing, LEITZ type, at 2 Kg load. The measurements were taken from five different indentations. Prior ferrite grain size measurements were carried out on five different images using the three circle technique [10].

Scanning Electron Microscope (SEM) TESCAN type, equipped with energy dispersive X ray (EDAX), was used to identify the microstructure of materials.

Tensile machine type of ZWICK, of 100 KN as a maximum load, was used with a deformation rate of 1mm/min piloted by PC. Specimens for tensile testing were machined from rods and each one have 150 mm of length with diameters of 6 mm and 3.18 mm for S1 and 5.5 mm and 3.25 mm for S2. Tensile tests are carried out at room temperature up to fracture.

Annealing of wiredrawing specimens were carried out at constant temperatures (500-510)°C for different holding times; samples were then quenched in water.

3. Results and discussion

3.1. Prior to wiredrawing

A homogenous and similar structure of equiaxed ferrite and pearlite for S1 and S2, before wiredrawing, is observed (Fig. 1).

The calculation of the pearlite percentage which is about 6.25% and 15.30% for S1 and S2 respectively confirms the low carbon content. The initial grain size of ferrite (d_{ini}) is found to be equal to 11 µm for both steels S1 and S2. The hardness is expected to indicate something about the strength of the material. The initial Vickers hardness of this structure increases with carbon content and other alloying elements and is about 120.4 Hv_2 and 175 Hv_2 for S1 and S2 respectively.

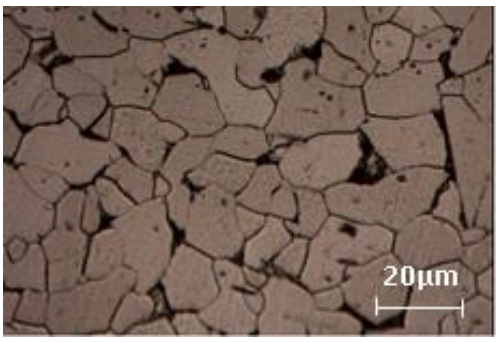

Figure 1. Typical optical microstructure of the S2 steel before wiredrawing.

It should be noted that the hardness of the material is controlled not only by the ferrite grain size and the percentage of the pearlite but also by the inter-lamellar spacing of pearlite. The inter-lamellar spacing of pearlite depends also on the cooling rate. When the cooling rate is rapid, the transformation of austenite to pearlite occurs at low temperature and a fine pearlite spacing results. The hardness is inversely proportional to the inter-lamellar spacing of pearlite [11]. It is necessary to recall that the alloying elements such as Mn and S allow the formation of

inclusions while others such as Cr and Mo with high content results in the formation of M_7C_3, M_2C, M_6C, carbides. However, the first type of carbide which is most usually found in low alloy carbon steels is M_3C (substitutional cementite). This carbide is an iron rich carbide and can take into solution appreciable amounts of elements such as Mn, Cr and Mo.

The deduced values of the $\alpha \leftrightarrow \gamma$ transformation temperatures, from dilatometer curves, are Ae_1 =740.5 °C, Ae_3 =849.5 °C and Ae_1 =727°C , Ae_3 =849°C for S1 and S2 respectively. These values show that the increase of carbon content and some other alloying elements does not play a significant role in changing Ae_1 and Ae_3. These results also suggest that the annealing temperature of deformed ferrite for the present steels has to be below Ae_1, so that two-phase ($\alpha + \gamma$) region can be prevented. It should be noted that for low carbon steels and low alloy steels, Ae_1 and Ae_3 temperatures can be calculated using empirical equations [12]. These equations relate the temperatures Ae_1 and Ae_3 to the chemical composition of steels. It is necessary to take care about the combined effect of alloying elements on Ae_1 and Ae_3. Some elements, such as carbon, decreases Ae_3 while others, such as Mo, increases Ae_3.

It is necessary to mention that wires, in as received condition, show the presence of inclusions and are flat/elongated at random directions (Fig. 2a and 2b). The microanalysis of inclusions shows that are oxide of iron containing about 30% wt Oxygen and 64% wt of Iron. Their presence is harmful to the wiredrawing process and reduces the ductility of the material [1].

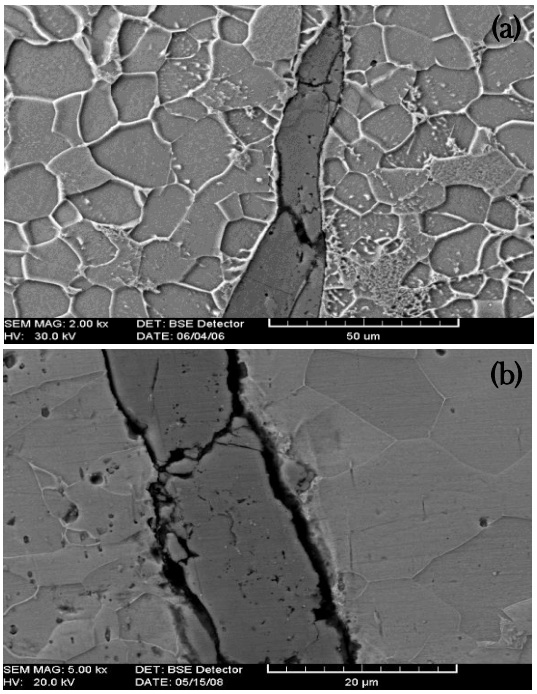

Figure 2. SEM micrographs showing inclusions: (a) S1 and (b) S2

Tensile tests for all specimens, in as received conditions, show essentially similar character. Tensile curves reveal the presence of the yield-point phenomena (or Lüders elongation-step III) (Fig.3), which is the characteristic of soft steels [1, 2, 13]. However, Tsuchida et al.[14] reported that Lüders elongation can be summarized only by the work-hardening rate for low carbon steels.

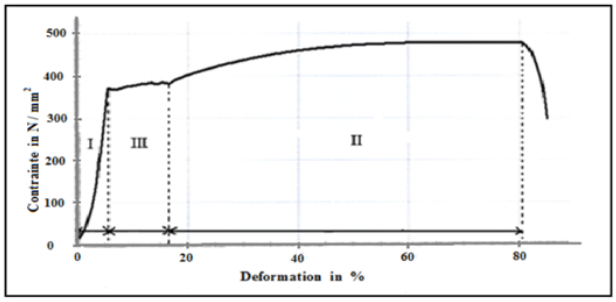

Figure 3: Typical curve of tensile test for S2 (ϕ = 5.5 mm) steel in as received conditions.

The results of mechanical properties are shown in table (2). It can be seen, as expected, that the tensile properties increase with carbon content and other alloying elements. Generally, hardness (H) is found to be three times greater than yield strength (Re) [13]. According to the value of ε_m, it is clear that the mechanical properties of both steels allow them to be used for further reduction of the area.

Table 2: Mechanical properties of tensile tests in as-received conditions of S1(ϕ=6.0 mm) and S2(ϕ=5.5 mm).

Steel	Hv (Kgf/mm²)	Re (N/mm²)	Rm (N/mm²)	ε_m (%)	ε_r (%)
S1	120.4	176.8	370.7	34	36.8
S2	175	368	480	73	77

Examination of fracture surfaces shows that the failure is characterized by the formation of the ductile voids with reduction in cross section. Figure 4 shows a typical fractured surface for S2.

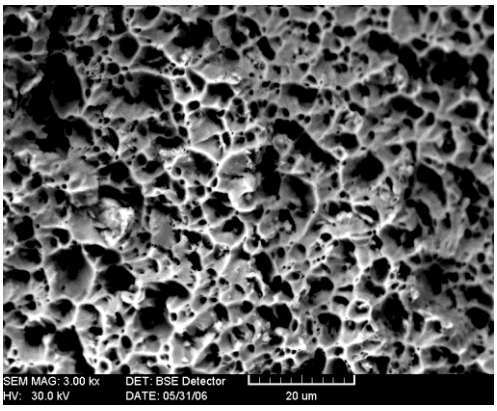

Figure 4. SEM micrograph of fractured surface for S2.

It can be seen that dimples have deep cavities which are not associated with particles or inclusions. Moreover, no

differences have been detected, in mode of fracture, between the two steels.

3.2. Post wiredrawing

However, both steels (i.e after reduction of area), have a homogenous structure of ferrite and pearlite and as a result of deformation the ferrite grains and pearlite are elongated in the direction of wiredrawing process for both steels and a typical optical structure for S2 steel is given in figure 5. When this structure is compared with the structure before wiredrawing, the observed variation is a direct consequence of the increase of dislocation density generated after the wiredrawing process.

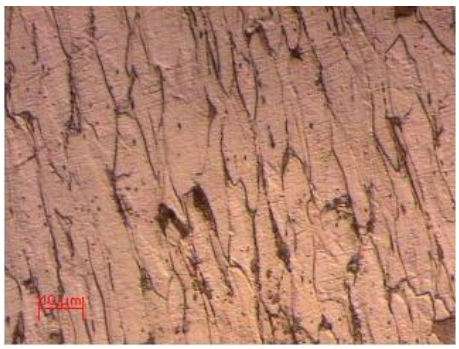

Figure 5. Typical optical microstructure of the S2 rod after wiredrawing.

It is necessary to note that the failure of wires after wiredrawing is still ductile characterized by cup-cone fracture. The results of mechanical properties after wiredrawing process are shown in table (3).

Table 3: Mechanical properties of tensile tests after wiredrawing of S1(φ=3.18mm) and S2(φ=3.25mm).

Steel	Hv (Kgf/mm²)	Re (N/mm²)	Rm (N/mm²)	ε_m (%)	ε_r (%)
S1	228	696.7	709.0	20.1	29
S2	248.4	775	816.5	19.5	21

It is clear that tensile properties, as it is expected, vary not only with the initial carbon content and other alloying elements but also with the effect of initial deformation rate. The high value of the deformation rate of S1 (72%) enhances the steel strength of S1 and reduces the differences in the yield strength between S1 and S2 due to the high content of carbon and other alloying elements in S2 steel. The combined effect of initial deformation rate and chemical composition has no apparent effect on the maximum deformation (ε_m) of both steels.

3.3. Primary recrystallization kinetics

Wiredrawing process followed by recrystallization is needed in order to soften the deformed material and to reach the equilibrium state. Primary recrystallization is a thermally activated process; the new grains (strain-free grains) nucleate and grow at the expense of the deformed ones.

The percentage of the new recrystallized grains (Xv) at 500°C as a function of holding times (t), using optical image analysis, is illustrated in figures 6a and 6b for S1 and S2, respectively.

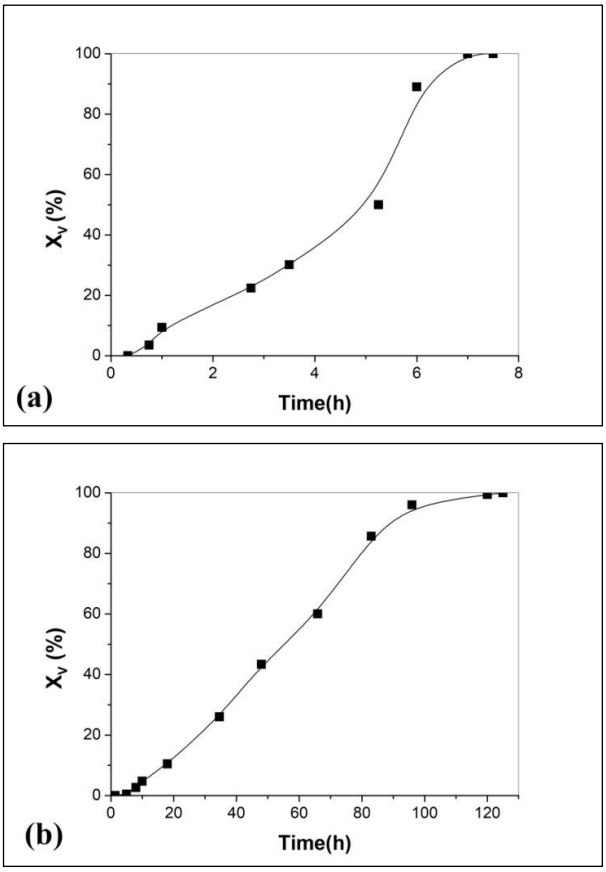

Figure 6. Recrystallized fraction (Xv) versus annealing time (t) at 500°C for : a) S1 and b) S2.

It can be seen that both steels follow the AVRAMI law:

$$Xv=1-\exp(-kt^n) \quad (1)$$

where n and k are constant which depend on the material and annealing temperature[4]. The values of n and k are deduced from the plot of ln(ln(1/(1-Xv))) against ln(t) for both steels (i.e JMAK plot). It is clear that the values of n and k of S1 steel are almost similar to those of S2 (Table 4).

Table 4: Values of n and k

steel	n	k
S1	1.52	0.019
S2	1.67	0.020

The annealing temperature of 500°C seems to be sufficient for the beginning of the primary recrystallization phenomenon, since these materials do not exhibit the

presence of the precipitates. Primary recrystallization times pass from t_s =0.347h and t_f= 7.638 h to t_s=5 h and t_f= 120 h for S1 and S2 respectively. It can be seen, from figure 6b that the nucleation period (where the nuclei form) is about 10 hours and then begin to grow at a constant rate of 1.08 h^{-1} up to 100 hours for S2 consuming the deformed matrix. However, for S1 the constant growing rate is higher and about 9.85 h^{-1} up to 5.25 hours than the growing rate rapidly increases to 27.621 h^{-1}. It is well known, that the primary recrystallization rate is influenced not only by the addition of alloying elements (drag effect) but also by the amount of deformation. The S2 steel, having more content carbon and (0.02%) Mo and deformed less (only by 65%), the recrystallization rate is significantly slowed. As the microstructure of deformed material is not well understood especially with the presence of second – phase; it is difficult to give a general assessment of recrystallization in inhomogeneous microstructure [7].

It is necessary to remember that the weak link between inclusions and matrix acts also as preferable sites for grain nucleation and growths, which enhances the nucleation rate of new grains. Figure 7 indicates clearly that the new grains (N.G) take place at the matrix/inclusion (inc.) interface. In spite of the wire (S1) is annealed at 510°C for only 5.3 hours ; it provides evidence that the matrix / inclusion interface are in favor of new grains nucleation during recrystallization.

The final recrystallized grain size at 500°C is almost similar, about 7 µm and 6.5 µm for S1 and S2 respectively. The corresponding Vickers hardness values after total recrystallization at 500°C are 110 Hv_2 and 174 Hv_2 for S1 and S2 respectively.

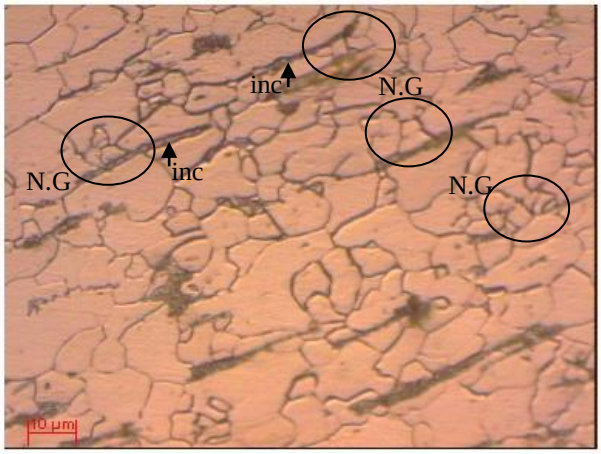

Figure 7. Typical optical micrograph showing the presence of new grains (N.G) at the matrix/inclusion interface for S1 steel annealed at 510°C for 5.3 hours.

3.4. Activation energy

The rate of primary recrystallization is given by Humpreys and Hathery [7] :

$$1/t_{1/2}=A \exp(-Q/RT) \quad (2)$$

Where A constant, R is rare gas constant and $t_{1/2}$ is the time for 50% of recrystallized grains at annealing temperature (T) and Q is the activation energy.

The present values of activation energy vary from 391.6 to 465.6 KJ mol^{-1} for S1 and S2 respectively. These values are higher than that for self-diffusion in α-iron (239.5 $KJmol^{-1}$) [2]. The higher activation energy determined for S2 steel may suggest that the increase in carbon content and alloying elements in S2 enhances the activation energy for primary recrystallization. It has been already demonstrated that the activation energy for primary recrystallization is lower for the highly deformed material [15]. It is necessary to remember that the rate of deformation of S2 (65%) is less than of S1 (72%) and there are differences in chemical composition between the two wires. As it has been explained earlier a proper comparison between S1 and S2 is not easy.

Finally, a correct comparison between the two wires necessitates a separation between the rate of deformation and the chemical composition.

4. Conclusion

The objectives of the present study and its achievements can be drawn as follow:

- The initial microstructure is ferrite-pearlite with 11µm of initial ferrite grain size for both steel S1 and S2. Moreover, both steels contain damaging inclusions rich in iron and oxygen.
- The wiredrawing process increases material strength and the failure of wires is ductile characterized by cup-cone fracture.
- It has been found that the primary recrystallization process at 500°C , for both steels, follow the Avrami law and the increase of carbon content has no effect on the two parameters n and k . The rate of primary recrystallization is significantly slowed down by the low deformation and the high carbon content of S2.
- The activation energy for primary recrystallization is found to be lower for the low carbon content steel and higher deformation rate.

Acknowledgments

The authors acknowledge financial support from the DGRSDT (MESRS-Algeria).

References

[1] G. E. Dieter, Mechanical Metallurgy, 3rd Edition , McGraw Hill book company, Singapore, 1986.
[2] J. Philibert, A. Vignes, Y. Bréchet, P. Combrade, du minerai au matériau, Ed. Masson, Paris,1998.
[3] B. Yalamanchili, P.M. Power, Dan. Lanham, Wire J. Int. 38 7 (2005) 108-113.
[4] M. Buršák, I. Mamuzić and J. Michel, Metalurgija 47 (2008) 19-23.

[5] I. Jandrli, S. Rešković, T. Brlić and V. Furlan, IOP Conf. Ser.: Mater. Sci. Eng. 461 (2019) 012030.
[6] W. Su-Fen, P. Yan and L. Zhi-Jie, Res. J. Apll. Sci. Eng. Technol. 5 (2013) 823.
[7] F.J. Humpreys, M. Hathery, Recrystallization and Related Phenomena, Pergamon Press, Oxford, 1995.
[8] L. Yaping, A. Dmitri, A. Molodov, G. Gottstein, Acta Materialia 59 (2011) 3229-3243.
[9] S.E. Hughes (ed), Quick Guide to Welding and Weld Inspection, Woodhead Publishing, UK, 2009, Ch.4.
[10] ASTM Standard Designation E112-88,1994, Book of ASTM standard, vol, 301, ASTM, Philadelphia, p227,(1997).
[11] C. Richardet, Structure et propriétés des Métaux, 2nd Edition, Dunod, 1970.
[12] D. Deng, Metals and Design 30 (2009) 359-366.
[13] M.F. Ashby and David R.H. Jones, Matériaux, 4th Edition, Dunod, Paris, 2008.
[14] N. Tsuchida, Y. Tomota, K. Naga, K. Fukaura, Scripta Materialia 54 (2006) 57-60.
[15] H. Bouhalais, Z. Larouk, Int. J. Microstructure and Materials Properties 6(5) (2011) 397-409.